

Microscopic predictions for production of neutron rich nuclei in the reaction $^{176}\text{Yb} + ^{176}\text{Yb}$

K. Godbey,^{1,*} C. Simenel,^{2,†} and A. S. Umar^{1,‡}

¹*Department of Physics and Astronomy, Vanderbilt University, Nashville, Tennessee 37235, USA*

²*Department of Theoretical Physics and Department of Nuclear Physics,
Research School of Physics, The Australian National University, Canberra ACT 2601, Australia*

(Dated: March 3, 2022)

Background: Production of neutron-rich nuclei is of vital importance to both understanding nuclear structure far from stability and to informing astrophysical models of the rapid neutron capture process (r-process). Multinucleon transfer (MNT) in heavy-ion collisions offers a possibility to produce neutron-rich nuclei far from stability.

Purpose: The $^{176}\text{Yb} + ^{176}\text{Yb}$ reaction has been suggested as a potential candidate to explore the neutron-rich region surrounding the principal fragments. The current study has been conducted with the goal of providing guidance for future experiments wishing to study this (or similar) system.

Methods: Time-dependent Hartree-Fock (TDHF) and its time-dependent random-phase approximation (TDRPA) extension are used to examine both scattering and MNT characteristics in $^{176}\text{Yb} + ^{176}\text{Yb}$. TDRPA calculations are performed to compute fluctuations and correlations of the neutron and proton numbers, allowing for estimates of primary fragment production probabilities.

Results: Both scattering results from TDHF and transfer results from the TDRPA are presented for different energies, orientations, and impact parameters. In addition to fragment composition, scattering angles and total kinetic energies, as well as correlations between these observables are presented.

Conclusions: $^{176}\text{Yb} + ^{176}\text{Yb}$ appears to be an interesting probe for the mid-mass neutron-rich region of the chart of nuclides. The predictions of both TDHF and TDRPA are speculative, and will benefit from future experimental results to test the validity of this approach to studying MNT in heavy, symmetric collisions.

I. INTRODUCTION

The synthesis of neutron-rich nuclei is one of the most exciting and challenging tasks in both experimental and theoretical nuclear physics. From the lightest systems to the superheavy regime, knowledge about the nuclei at the extremes of the chart of nuclides is vital to understanding physical phenomena at multiple scales. At the foremost, neutron-rich nuclei are at the literal and figurative center of the rapid neutron capture process (r-process). Attempts at modeling the r-process utilize input from nuclear models to inform threshold energies for the reaction types that characterize this process [1]. Thus, strong theoretical understanding of both the static and dynamic properties of nuclei far from stability can give vital insight into the formation of stable heavy nuclei.

The production of neutron-rich nuclei is also of interest for studying nuclear structure, where exploring this region of the nuclear landscape clearly probes the edges of our current understanding of how finite nuclei form and are composed [2]. This includes studies of neutron-rich nuclei of all masses, ranging from oxygen [3] up to the superheavy element (SHE) region. SHEs are of particular note, as the formation and static properties of said nuclei have been the focus of many experimental [4–8] and theoretical [9–13] studies.

Over the years, many theoretical approaches to studying neutron-rich nuclei formation have been pursued for various reaction types. One such technique is to use models to study

neutron enrichment via multinucleon transfer (MNT) in deep-inelastic collisions (DIC) and quasifission reactions [14–22]. While quasifission occurs at a much shorter time-scale than fusion-fission [23,24] and is the primary reaction mechanism that limits the formation of superheavy nuclei, the fragments produced may still be neutron-rich.

Quasifission reactions are often studied in asymmetric systems with, e.g., an actinide target [23,25–28]. However, quasifission can also be present in symmetric systems. In fact, the extreme case of quasifission in actinide-actinide collisions has been suggested as a possible reaction mechanism to obtain neutron-rich isotopes of high Z nuclei in particular as well as a possible means to search for SHE [29,30]. Theoretically, the investigation of actinide-actinide collisions has a rich history with various approaches, including the dinuclear system (DNS) model [31], relativistic mean-field (RMF) and Skyrme HF studies [32], reduced density-matrix formalism [33], quantum molecular dynamics (QMD) [34], and improved quantum molecular dynamics (ImQMD) [20,35] calculations, as well as time-dependent Hartree-Fock (TDHF) studies [17,19,36]. Over recent years, TDHF has proved to be a tool of choice to investigate fragment properties produced in various reactions, such as DIC [22,37], quasifission [21, 28,38–42], and fission [43–52]. Recent reviews [53,54] succinctly summarize the current state of TDHF (and its extensions) as it has been applied to various MNT reactions.

In this work, we present a study of the $^{176}\text{Yb} + ^{176}\text{Yb}$ system using TDHF and the time-dependent random phase approximation (TDRPA) extension that considers the effect of one-body fluctuations around the TDHF trajectory. As discussed before, microscopic approaches such as TDHF and its extensions are commonly used in heavy-ion collision studies in different regions of the nuclear chart, positioning TDHF

* kyle.s.godbey@vanderbilt.edu

† cedric.simenel@anu.edu.au

‡ umar@compsci.cas.vanderbilt.edu

and TDRPA as tools of choice for the current investigation. Symmetric ^{176}Yb reactions were chosen because they are considered as a potential candidate to explore the neutron-rich region around the mass region $A \sim 170 - 180$ of the nuclear chart. Specifically, an experimental investigation of this reaction are being considered in Dubna by Oganessian *et al.* and the work presented here was undertaken at their suggestion [55]. The base theory (TDHF) and the primary extension (TDRPA) are briefly described in Section II. Results for both scattering characteristics and transfer characteristics are discussed in Section III A and Section III B respectively. A summary and outlook are then presented in Section IV.

II. FORMALISM: TDHF AND TDRPA

The TDHF theory provides a microscopic approach with which one may investigate a wide range of phenomena observed in low energy nuclear physics [53,54,56,57]. Specifically, TDHF provides a dynamic quantum many-body description of nuclear reactions in the vicinity of the Coulomb barrier, such as fusion [58–73] and transfer reactions [16,37,54,74–80].

The TDHF equations for the single-particle wave functions

$$h(\{\phi_\mu\}) \phi_\lambda(r, t) = i\hbar \frac{\partial}{\partial t} \phi_\lambda(r, t) \quad (\lambda = 1, \dots, A), \quad (1)$$

can be derived from a variational principle. The principal approximation in TDHF is that the many-body wave function $\Phi(t)$ is assumed to be a single time-dependent Slater determinant at all times. It describes the time-evolution of the single-particle wave functions in a mean-field corresponding to the dominant reaction channel. During the past decade it has become numerically feasible to perform TDHF calculations on a 3D Cartesian grid without any symmetry restrictions and with much more accurate numerical methods [77,81–83].

The main limitation in the TDHF theory when studying features like particle transfer, however, is that it is optimized for the prediction of expectation values of one-body observables [84] and will under-predict fluctuations of those observables [85]. This is due to the fact that the fluctuation of one-body operators (such as the particle number operator) includes the expectation value of the square of a one-body operator,

$$\sigma_{XX} = \sqrt{\langle \hat{X}^2 \rangle - \langle \hat{X} \rangle^2}, \quad (2)$$

that is outside the variational space of TDHF [84].

To obtain such quantities one needs to go beyond standard TDHF and consider the fluctuations around the TDHF mean-field trajectory using techniques like the stochastic mean-field theory [86,87] or TDRPA [88], which has recently been used to investigate DIC [76,89,90]. In this work we follow a similar approach as in [76,90] to obtain particle number fluctuations and distributions about the outgoing fragments.

The procedure to obtain the desired correlations involves first transforming the states after the collision as

$$\tilde{\phi}_\alpha^X(r, t_f) = \exp[-i\varepsilon N_X \Theta_V(r)] \phi_\alpha(r, t_f), \quad (3)$$

where X stands for neutron (N), proton (Z), or total nucleon number (A). The operator N_X ensures that the transformation acts only on nucleons with the correct isospin, with $N_A = 1$, $N_Z = \frac{1-\tau_3}{2}$, and $N_N = \frac{1+\tau_3}{2}$. The operator $\Theta_V(\hat{r})$ is a step function that is either 1 or 0 depending on whether r is within a volume of space, V , delimiting the fragment of interest. Finally, ε is a small number that is varied to achieve convergence.

These transformed states are then propagated backwards in time from the final time t_f to the initial time t_i . The correlations can then be calculated by evaluating

$$\sigma_{XY} = \sqrt{\lim_{\varepsilon \rightarrow 0} \frac{\eta_{00} + \eta_{XY} - \eta_{0X} - \eta_{0Y}}{2\varepsilon^2}}, \quad (4)$$

with η_{XY} describing the overlap between the states at time $t = t_i$,

$$\eta_{XY} = \sum_{\alpha\beta} \left| \langle \phi_\alpha^X(t_i) | \phi_\beta^Y(t_i) \rangle \right|^2. \quad (5)$$

In the case of $X, Y = 0$, this refers to states obtained with $\varepsilon = 0$ in Eq. (3). In principle, one should recover exactly the initial state as the evolution is unitary. However, using states that have been evolved forward and then backward in time with $\varepsilon = 0$ minimizes systematic errors from numerical inaccuracies [89,91].

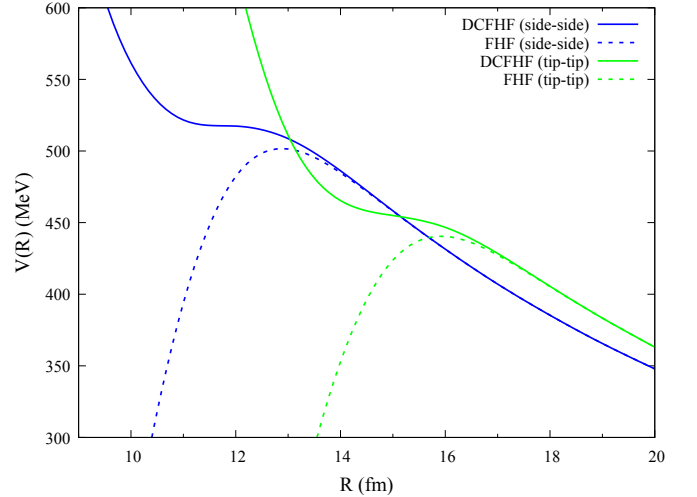


FIG. 1. (Color online). Static nuclear potentials for $^{176}\text{Yb} + ^{176}\text{Yb}$ in the side-side (blue (dark) lines) and tip-tip (green (light) lines) orientations from FHF and DCFHF.

The SLy4d parametrization of the Skyrme functional is used [92] and all calculations were performed in a numerical box with 66×66 points in the reaction plane, and 36 points along the axis perpendicular to the reaction plane. The grid spacing used was a standard 1.0 fm which provides an excellent numerical representation of spatial quantities using the basis spline collocation method [93]. For the TDRPA calculations, each initial orientation, energy, and impact parameter resulted in three additional TDHF evolutions (one for each X) for the time reversed evolution at one value of $\varepsilon = 2 \times 10^{-3}$ in addition to occasionally scanning ε to ensure convergence

of Eq. (4). In total, 200 full TDHF evolutions were required for the results presented in this work with each taking on the order of $10 \sim 55$ hours of wall time due to the large, three-dimensional box size chosen. This corresponds to roughly 250 days of computation time split among multiple nodes for the ^{176}Yb HF ground state configuration with a prolate deformation.

The proton and neutron numbers correlations and fluctuations computed with TDRPA are used to estimate probabilities for the formation of a given nuclide using Gaussian bivariate normal distributions of the form

$$\mathcal{P}(n, z) = \mathcal{P}(0, 0) \exp \left[-\frac{1}{1 - \rho^2} \left(\frac{n^2}{\sigma_{NN}^2} + \frac{z^2}{\sigma_{ZZ}^2} - \frac{2\rho n z}{\sigma_{NN}\sigma_{ZZ}} \right) \right], \quad (6)$$

where n and z are the number of transferred neutrons and protons, respectively. The correlations between N and Z are quantified by the parameter

$$\rho = \text{sign}(\sigma_{NZ}) \frac{\sigma_{NZ}^2}{\sigma_{NN}\sigma_{ZZ}} = \frac{\langle n z \rangle}{\sqrt{\langle n^2 \rangle \langle z^2 \rangle}}. \quad (7)$$

In principle, n and z could be very large and lead to unphysical predictions with fragments having, e.g., a negative number of protons and neutrons, or more nucleons than available. In practice, such spurious results could only happen for the most violent collisions where the fluctuations are large. To avoid such spurious effects, the probabilities are shifted so that \mathcal{P} is zero when one fragment has all (or more) protons or neutrons. The resulting distribution is then normalized.

Although the ^{176}Yb nuclide is in a region where shape coexistence is often found [94–98], TDHF calculations can only be performed with one well-defined deformation (and orientation) of each collision partners in the entrance channel. In our calculations, the ground state is found to have a prolate deformation with $\beta_2 \simeq 0.33$ in its HF ground state. A higher energy oblate solution is also found with a difference of around 5 MeV in total binding energy. A set of calculations were also performed for the oblate solution, though the overall transfer behavior was found to be similar for both deformations despite the oblate one resulting in slightly lower fluctuations. In the following, we thus only show results for the prolate ground state.

This deformation allows for possible choices of the orientation of the nuclei. Extreme orientations are called “side” (“tip”) when the deformation axis is initially perpendicular (parallel) to the collision axis. Although various intermediate orientations could be considered [42], we limit our study to tip-tip and side-side orientations where the initial orientations of both nuclei are identical. In addition to saving computational time, this restriction is necessary to ensure fully symmetric collisions and to avoid unphysical results in TDRPA [90].

Figure 1 shows the nucleus-nucleus potentials computed using the frozen Hartree-Fock (FHF) [62,99] and density-constrained frozen Hartree-Fock (DCFHF) [100] methods, respectively neglecting and including the Pauli exclusion principle between the nucleons of different nuclei. Due to Pauli

repulsion in DCFHF, the inner pocket potential is very shallow in the side-side configuration, and disappears in the tip-tip one. In this work, the effect of the orientation is studied by comparing tip-tip and side-side configurations at a center of mass energy $E_{\text{c.m.}} = 660$ MeV. In addition, calculations are also performed at $E_{\text{c.m.}} = 880$ MeV for both orientations to investigate the role of the energy on the reaction outcome.

III. RESULTS

In this section we present the results of TDHF and TDRPA studies of $^{176}\text{Yb} + ^{176}\text{Yb}$ reactions at different center of mass energies and initial orientations for a range of impact parameters. Both scattering features and particle number fluctuation derived quantities were calculated and are shown below.

A. Scattering Characteristics

The following section presents scattering results from the standard TDHF calculations of $^{176}\text{Yb} + ^{176}\text{Yb}$ collisions. The TDRPA extension to TDHF is not needed for these results, though this means the points can only be interpreted as the most likely outcome for each initial condition.

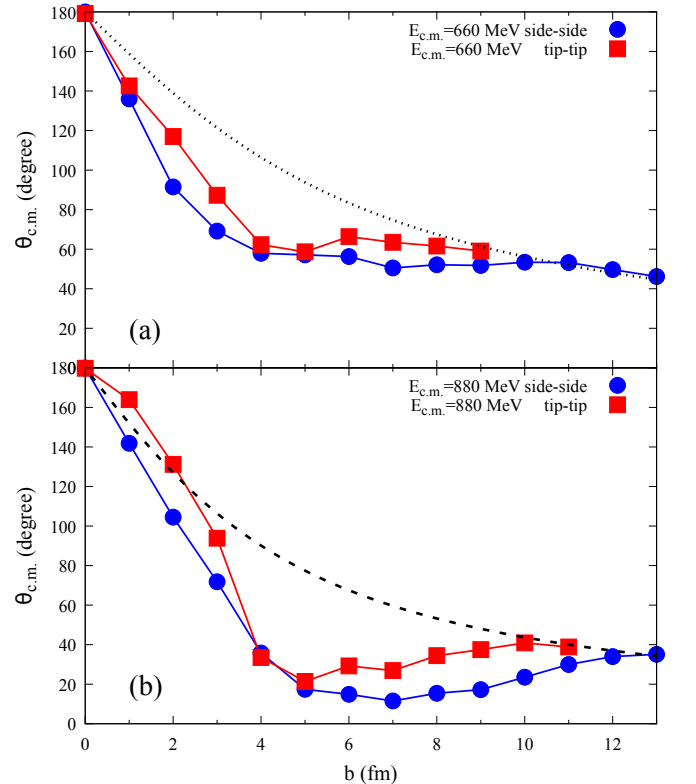


FIG. 2. (Color online). Scattering angles for $^{176}\text{Yb} + ^{176}\text{Yb}$ collisions at center of mass energies (a) $E_{\text{c.m.}} = 660$ MeV and (b) $E_{\text{c.m.}} = 880$ MeV in the side-side (circles) and tip-tip (squares) orientations. The dotted (dashed) line plots the Rutherford scattering angle for $E_{\text{c.m.}} = 660$ MeV (880 MeV).

Scattering angles for the $^{176}\text{Yb} + ^{176}\text{Yb}$ system for both orientations are presented in Fig. 2. A similar deviation from Rutherford scattering is observed at impact parameters $b \leq 8$ fm for both orientations. These deviations are due to nuclear deflection and partial orbiting of the system. Note that no fusion is observed. The relatively flat shape of the curve around $50 - 60^\circ$ at 660 MeV and $20 - 40^\circ$ at 880 MeV implies a large number of events in these particular angular ranges.

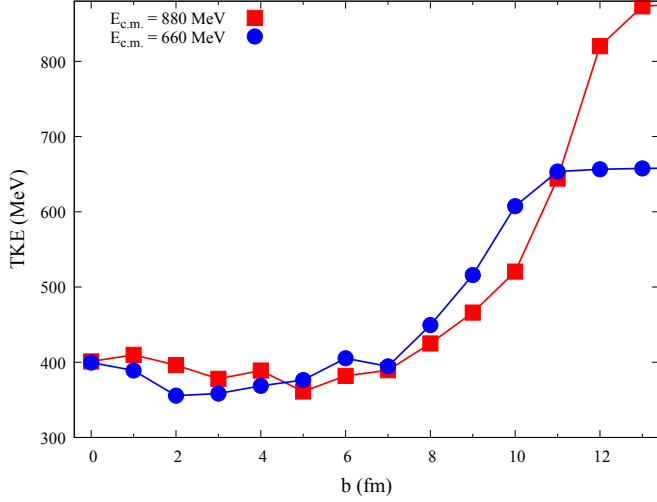


FIG. 3. (Color online). Total kinetic energies of the outgoing fragments in $^{176}\text{Yb} + ^{176}\text{Yb}$ collisions at center of mass energies $E_{c.m.} = 660$ MeV (blue circles) and $E_{c.m.} = 880$ MeV (red squares) in the side-side orientation.

The TKE of the outgoing fragments is plotted in Fig. 3 as a function of the impact parameter b for side-side collisions at the two center of mass energies. Although dissipation occurs at different impact parameter ranges ($b < 10$ fm at $E_{c.m.} = 660$ MeV and $b < 12$ fm at $E_{c.m.} = 880$ MeV), both curves exhibit similar behavior. In particular, the TKEs saturate at roughly the same energy ($\sim 350 - 400$ MeV) indicating full damping of the initial TKE for the most central collisions.

Among the mechanisms responsible for energy dissipation, nucleon transfer is expected to play an important role. Of course, in symmetric collisions the average number of nucleons in the fragments does not change. Nevertheless, multi-nucleon transfer is possible thanks to fluctuations, leading to finite widths in the fragment particle number distributions. These fluctuations are explored in the following section.

B. Transfer Characteristics

This section focuses on the results obtained by extending TDHF to recover particle number fluctuations and correlations with the TDRPA.

Particle number fluctuations (σ_{ZZ} and σ_{NN}) and correlations (σ_{NZ}) calculated from Eq. (4) are shown in Fig. 4 as a function of impact parameters for different initial conditions. The fluctuations are greater in general at the smaller impact

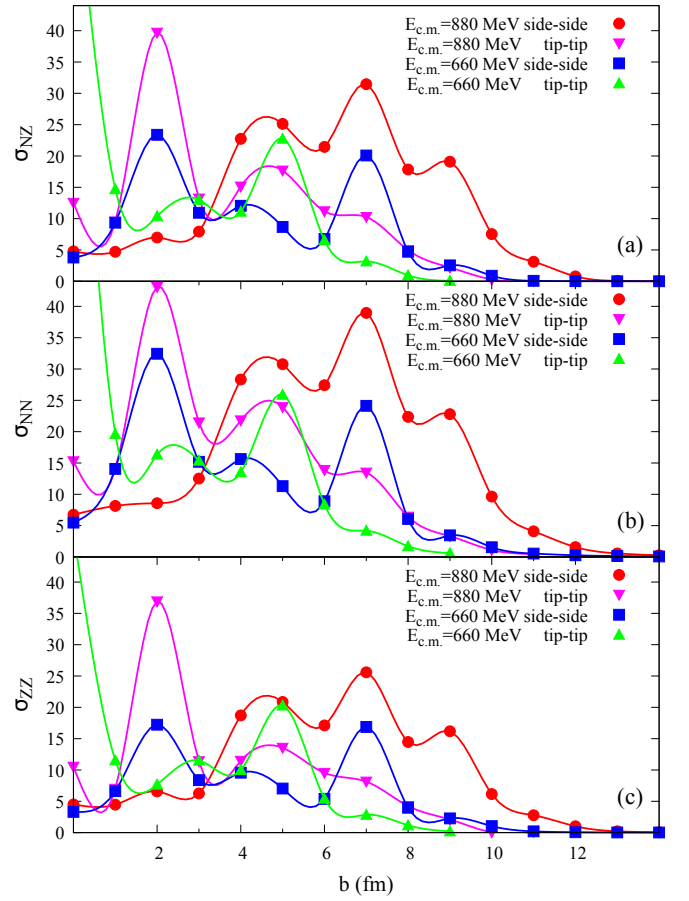


FIG. 4. (Color online). TDRPA predictions of correlations σ_{NZ} (a) and fluctuations σ_{NN} (b) and σ_{ZZ} (c) for $^{176}\text{Yb} + ^{176}\text{Yb}$ collisions for four initial configurations over a range of impact parameters.

parameters, though they do not converge to a single value. Similar variations in fluctuations were already observed in earlier TDRPA studies of deep inelastic collisions in lighter systems [76,90]. Particularly large values are sometimes obtained, such as at 660 MeV in tip-tip central ($b = 0$) collisions, indicating approximately flat distributions around the TDHF average.

Fragment mass-angle distributions (MADs) are a standard tool used experimentally to interpret the dynamics of heavy-ion collisions [23,28,39,101–107]. Although TDHF has been used to help interpret theoretically these distributions [28,39,41,108], these earlier calculations only incorporate fluctuations coming from the distribution of initial conditions (e.g., different orientations). Here, we go beyond the mean-field prediction by including the fragment mass fluctuations from TDRPA. Note that we only include mass fluctuations, not fluctuations in scattering angle which are still determined solely by TDHF. Calculating quantum fluctuations of scattering angles is beyond the scope of this work, although they might be necessary for a more detailed comparison with experimental MADs.

The resulting MADs for $^{176}\text{Yb} + ^{176}\text{Yb}$ reactions are shown in Fig. 5. The mass ratio M_R is defined as the ratio of the

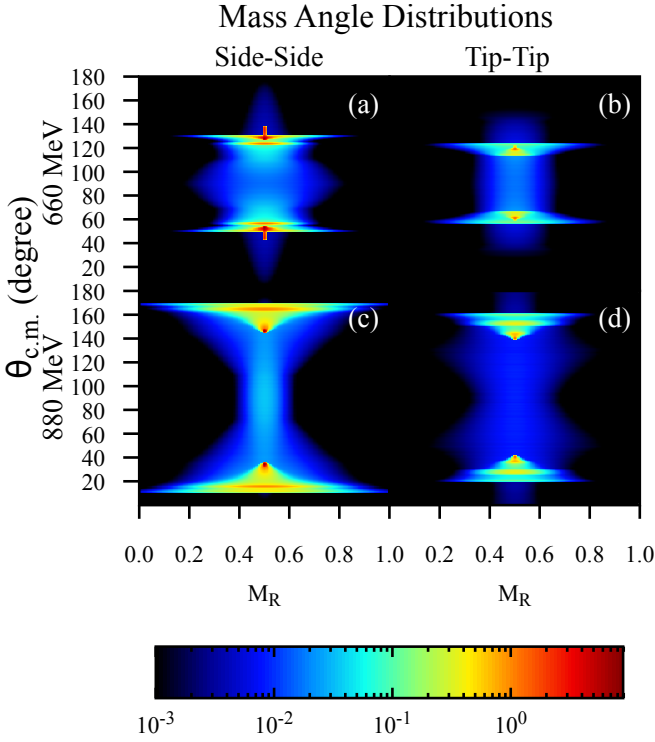


FIG. 5. (Color online). Mass angle distributions for $^{176}\text{Yb} + ^{176}\text{Yb}$ collisions at (a) $E_{c.m.} = 660$ MeV in the side-side orientation, (b) $E_{c.m.} = 660$ MeV in the tip-tip orientation, (c) $E_{c.m.} = 880$ MeV in the side-side orientation, and (d) $E_{c.m.} = 880$ MeV in the tip-tip orientation. The colorbar represents cross sections in millibarns per bin of mass ratio and degree.

fragment mass over the total mass of the system. The distributions of mass ratios are determined assuming Gaussian distributions with standard deviation $\sigma_{M_R} = \sigma_{AA}/A$, limited and normalized to the physical region $0 \leq M_R \leq 1$ (see section II). There is then an M_R distribution per initial condition (defined by $E_{c.m.}$, b , and the orientations), but only a single scattering angle $\theta_{c.m.}$. To obtain a continuous representation of the scattering angle, $\theta_{c.m.}$ is discretized into bins of $\Delta\theta = 1$ degree and interpolated between the values obtained by TDHF.

The figures are symmetric about 90° as both outgoing fragments are identically the same and will then travel outwards at complimentary angles. Specific orientations such as side-side and tip-tip will not be accessible in an experimental setting of course. Interestingly, when investigating initial energy dependence of the MAD (compare panels (a) and (c), (b) and (d) in Fig. 5), it can be seen that different outgoing angles are preferred depending on the incoming center of mass energy with back (and forward) scattering events being more prevalent in the higher energy regime.

This agrees well with what is seen in Fig. 2, where many impact parameters result in scattering angles around $50 - 60$ degrees at $E_{c.m.} = 660$ MeV and around $20 - 40$ degrees at 880 MeV. This is the case for both tip-tip and side-side orientations, though the tip-tip results tend further towards the intermediate angles than side-side at the same energy.

While the predictive capability of this method needs to be

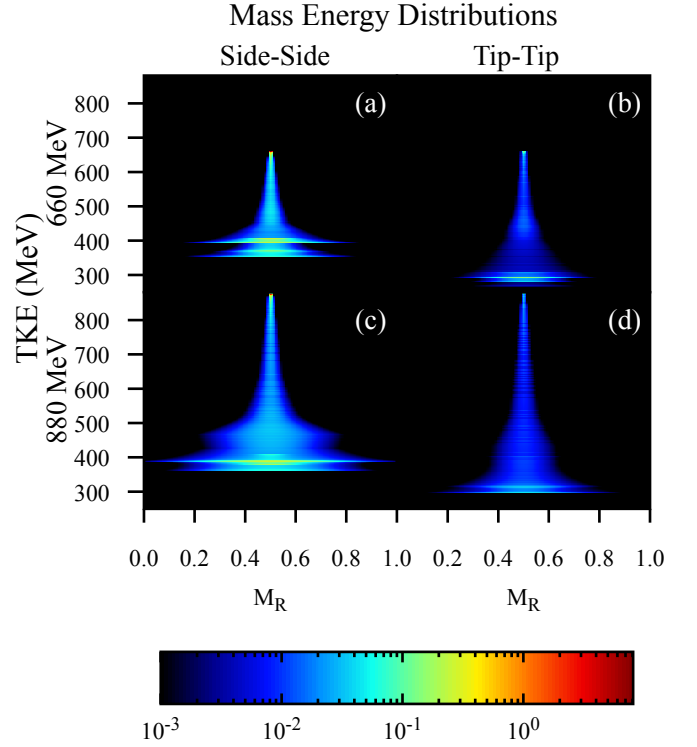


FIG. 6. (Color online). Mass energy distributions for $^{176}\text{Yb} + ^{176}\text{Yb}$ collisions at (a) $E_{c.m.} = 660$ MeV in the side-side orientation, (b) $E_{c.m.} = 660$ MeV in the tip-tip orientation, (c) $E_{c.m.} = 880$ MeV in the side-side orientation, and (d) $E_{c.m.} = 880$ MeV in the tip-tip orientation. The colorbar represents cross sections in millibarns per bin of mass ratio and MeV.

compared with experimental results and tested, this suggests a strong energy dependence and that detection of fragment production will greatly benefit from large angle detectors. The energy dependence seen in the MAD is not intuitive, and may prove to be useful for informing experimental setups.

Useful information can also be obtained from the correlations between fragment mass and kinetic energy [27,110–113]. Figure 6 presents mass energy distributions (MED) that detail the predicted TKE of outgoing fragments. It should be noted here that, while the theory provides particle number fluctuations, the values for TKE are single points (as in the case of $\theta_{c.m.}$) as predicted by TDHF alone. That is, widths of the TKE distributions are currently unknown with the method used here. This would make for an excellent extension to the theory, bringing it more in line with what can be experimentally observed.

The MEDs exhibit a continuous broadening of the mass distribution with increasing energy dissipation. The saturation of TKE lies around $350 - 400$ MeV for side-side collisions (see also Fig. 3) and around $250 - 300$ MeV for tip-tip. This difference between orientations is interesting as it indicates a larger kinetic energy dissipation with less compact configurations. A possible explanation is that the nuclei overlap at a larger distance in the tip-tip configuration, thus producing energy dissipation earlier in the collision process than in the side-side orientation.

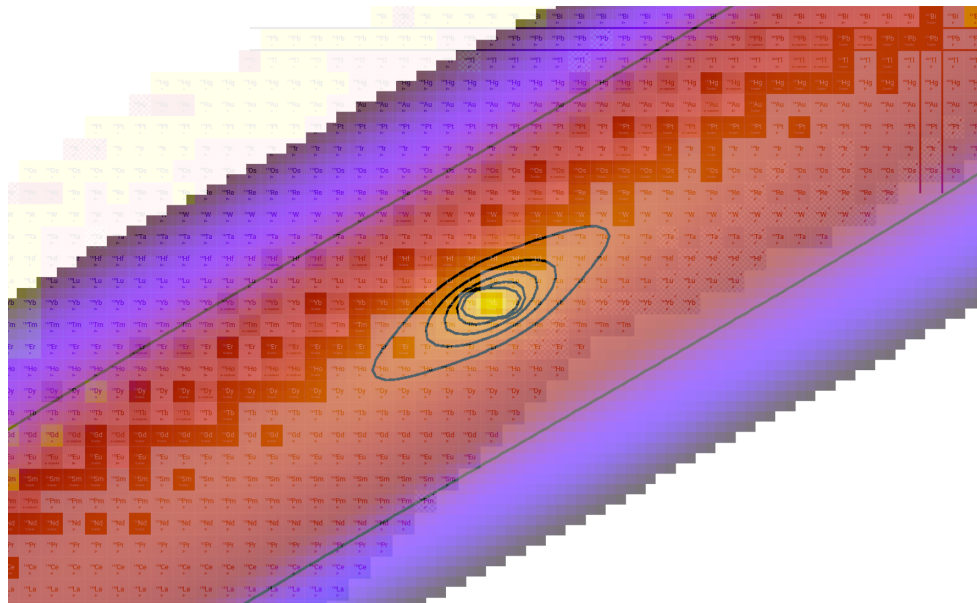


FIG. 7. (Color online). Primary fragments production cross sections for $^{176}\text{Yb} + ^{176}\text{Yb}$ collisions at $E_{c.m.} = 660$ MeV in the side-side orientation overlaid onto the chart of nuclides. The innermost contour corresponds to a cross section of 1 millibarn, with subsequent contours drawn every 0.2 mb. Finally, we also plot a boundary contour drawn at the microbarn level. Chart from [109].

In general, the MEDs show peaks around the elastic and fully damped regions which results from the large range of impact parameters contributing to both mechanisms.

C. Primary fragments production

Using the correlations and fluctuations shown in Fig. 4, a map of probabilities can be made in the N - Z plane assuming a modified Gaussian bivariate normal distribution (See section II and Eq. (6)). This choice of using a Gaussian is the primary assumption when calculating probabilities and related quantities and may not accurately describe the true distribution far from the center.

These probability distributions at multiple impact parameters can then be integrated over to produce a map of primary fragment production cross sections which is presented in Fig. 7 overlaid atop a section of the chart of nuclides in the region surrounding ^{176}Yb [109]. As the probability distributions for each impact parameter will be centered around the ^{176}Yb ($Z = 70$, $N = 106$) nuclide, the resulting cross sections are also symmetric about ^{176}Yb . The inclusion of correlations between protons and neutrons via σ_{NZ} more or less aligns the distribution parallel to the valley of stability due to the symmetry energy.

Subsequent decay of the fragments would inevitably bring the final products closer to the valley of stability. Here, our focus is on primary fragment productions and the prediction of evaporation residue cross-sections are beyond the scope of this work. In fact, experimental measurements of mass-angle distributions using time of flight techniques are for primary fragments as they assume two-body kinematics [114]. To estimate the evaporation residue cross-sections would require to

first compute the excitation energy of the fragments and then predict their decay with a statistical model [37,115].

One way to minimize evaporation is to consider less violent collisions. In terms of primary fragment productions, 660 and 880 MeV center of mass energies are quite similar (this can be seen by the relatively similar particle number fluctuations in Fig. 4). However, the higher energy will lead to more neutron evaporation and thus to less exotic evaporation residues. Use of relatively neutron-rich ^{176}Yb nuclei in symmetric collisions may then allow for this reaction to act as a probe of the neutron-rich region surrounding the principal outgoing fragment.

IV. SUMMARY AND DISCUSSION

Multiple TDHF and TDRPA calculations have been performed for the $^{176}\text{Yb} + ^{176}\text{Yb}$ system with various initial orientations, energies, and impact parameters. Standard TDHF allows for the classification of general scattering characteristics, while the TDRPA technique extends the approach to include correlations and fluctuations of particle numbers of the reaction fragments. This extension provides a theoretical framework that more closely resembles what will be seen in experimental investigations of this (and similar) systems.

In examining figures such as the mass-angle distributions in Fig. 5, information regarding the angular distribution of fragments can be gleaned and suggest large acceptance detectors to maximize measurement capability. Mass-energy distributions shown in Fig. 6 are also useful to investigate, e.g., the interplay between dissipation and fluctuations. In both cases, however, fluctuations of $\theta_{c.m.}$ and of TKE are not predicted in the present study. The latter would require new implemen-

tations of the TDRPA to these observables, or the use of alternative approaches such as the stochastic mean-field theory [49] or an extension of the Langevin equation [116]. Both methods have been recently used to investigate kinetic energy distributions in fission fragments. In order to benchmark our theoretical methods as applied to symmetric heavy nuclei, all predictions presented in this study would greatly benefit from experimental verification.

The methods used here provide a very powerful tool for investigating symmetric systems, though an important caveat should be discussed regarding the interpretation of these results. TDRPA produces only correlations and fluctuations, not the actual distributions themselves, which are then taken to be of a Gaussian nature. This assumption may break down when far from the center of the distribution or if the shape at the center itself is too flat and deviates sufficiently from a Gaussian behavior. It is then extremely important to compare with observations made in experimental studies such that we may better understand how to interpret the results coming from these methods.

Regardless, the $^{176}\text{Yb} + ^{176}\text{Yb}$ system presents itself as a viable candidate for studies of MNT processes and production of neutron rich nuclei in the region around $A \sim 176$. The map of possible primary fragments loosely painted in Fig. 7 presents an exciting range of previously inaccessible nuclei, with the above caveat applying the further one goes from the center of the distribution. Another caveat is that the predicted distribution is for primary fragments only and that statistical decay should be included in order to predict fragment produced after evaporation, e.g., following [22,37,115].

ACKNOWLEDGMENTS

We thank Yu. Ts. Oganessian and D. J. Hinde for stimulating discussions. This work has been supported by the U.S. Department of Energy under grant No. DE-SC0013847 with Vanderbilt University and by the Australian Research Councils Grant No. DP190100256.

-
- [1] J. J. Cowan, C. Sneden, J. E. Lawler, A. Aprahamian, M. Wiescher, K. Langanke, G. Martínez-Pinedo, and F.-K. Thielemann, Making the Heaviest Elements in the Universe: A Review of the Rapid Neutron Capture Process, [Arxiv:1901.01410](#) (2019).
 - [2] T. Otsuka, A. Gade, O. Sorlin, T. Suzuki, and Y. Utsuno, Evolution of nuclear structure in exotic nuclei driven by nuclear forces, [Arxiv:1805.06501](#) (2018), accepted in *Rev. Mod. Phys.*
 - [3] R. T. deSouza, S. Hudan, V. E. Oberacker, and A. S. Umar, Confronting measured near- and sub-barrier fusion cross sections for $^{20}\text{O} + ^{12}\text{C}$ with a microscopic method, *Phys. Rev. C* **88**, 014602 (2013).
 - [4] S. Hofmann, F. P. Heßberger, D. Ackermann, G. Münzenberg, S. Antalic, P. Cagarda, B. Kindler, J. Kojouharova, M. Leino, B. Lommel, R. Mann, A. G. Popeko, S. Reshitko, S. Šaro, J. Uusitalo, and A. V. Yeremin, New results on elements 111 and 112, *Eur. Phys. J. A* **14**, 147 (2002).
 - [5] G. Münzenberg and K. Morita, Synthesis of the heaviest nuclei in cold fusion reactions, *Nucl. Phys. A* **944**, 3 (2015).
 - [6] K. Morita, SHE research at RIKEN/GARIS, *Nucl. Phys. A* **944**, 30 (2015).
 - [7] Yu. Ts. Oganessian and V. K. Utyonkov, Superheavy nuclei from ^{48}Ca -induced reactions, *Nucl. Phys. A* **944**, 62 (2015).
 - [8] J. B. Roberto, C. W. Alexander, R. A. Boll, J. D. Burns, J. G. Ezold, L. K. Felker, S. L. Hogle, and K. P. Rykaczewski, Actinide targets for the synthesis of super-heavy elements, *Nucl. Phys. A* **944**, 99 (2015).
 - [9] M. Bender, K. Rutz, P.-G. Reinhard, J. A. Maruhn, and W. Greiner, Shell structure of superheavy nuclei in self-consistent mean-field models, *Phys. Rev. C* **60**, 034304 (1999).
 - [10] W. Nazarewicz, M. Bender, S. Ćwiok, P. H. Heenen, A. T. Kruppa, P.-G. Reinhard, and T. Vertse, Theoretical description of superheavy nuclei, *Nucl. Phys. A* **701**, 165 (2002).
 - [11] S. Ćwiok, P.-H. Heenen, and W. Nazarewicz, Shape coexistence and triaxiality in the superheavy nuclei, *Nature* **433**, 705 (2005).
 - [12] J. C. Pei, W. Nazarewicz, J. A. Sheikh, and A. K. Kerman, Fission Barriers of Compound Superheavy Nuclei, *Phys. Rev. Lett.* **102**, 192501 (2009).
 - [13] J. R. Stone, K. Morita, P. A. M. Guichon, and A. W. Thomas, Physics of even-even superheavy nuclei with $96 < Z < 110$ in the quark-meson-coupling model, *Phys. Rev. C* **100**, 044302 (2019).
 - [14] G. G. Adamian, N. V. Antonenko, and W. Scheid, Characteristics of quasifission products within the dinuclear system model, *Phys. Rev. C* **68**, 034601 (2003).
 - [15] Valery Zagrebaev and Walter Greiner, Shell effects in damped collisions: a new way to superheavies, *J. Phys. G* **34**, 2265 (2007).
 - [16] A. S. Umar, V. E. Oberacker, and J. A. Maruhn, Neutron transfer dynamics and doorway to fusion in time-dependent Hartree-Fock theory, *Eur. Phys. J. A* **37**, 245 (2008).
 - [17] Cédric Golabek and Cédric Simenel, Collision Dynamics of Two ^{238}U Atomic Nuclei, *Phys. Rev. Lett.* **103**, 042701 (2009).
 - [18] Y. Aritomo, Analysis of dynamical processes using the mass distribution of fission fragments in heavy-ion reactions, *Phys. Rev. C* **80**, 064604 (2009).
 - [19] David J. Kedziora and Cédric Simenel, New inverse quasifission mechanism to produce neutron-rich transfermium nuclei, *Phys. Rev. C* **81**, 044613 (2010).
 - [20] K. Zhao, Z. Li, Y. Zhang, N. Wang, Q. Li, C. Shen, Y. Wang, and X. Wu, Production of unknown neutron-rich isotopes in $^{238}\text{U} + ^{238}\text{U}$ collisions at near-barrier energy, *Phys. Rev. C* **94**, 024601 (2016).
 - [21] K. Sekizawa, Enhanced nucleon transfer in tip collisions of $^{238}\text{U} + ^{124}\text{Sn}$, *Phys. Rev. C* **96**, 041601 (2017).
 - [22] Z. Wu and L. Guo, Microscopic studies of production cross sections in multinucleon transfer reaction $^{58}\text{Ni} + ^{124}\text{Sn}$, *Phys. Rev. C* **100**, 014612 (2019).
 - [23] J. Töke, R. Bock, G. X. Dai, A. Gobbi, S. Gralla, K. D. Hildenbrand, J. Kuzminski, W. F. J. Müller, A. Olmi, H. Stelzer, B. B.

- Back, and S. Bjørnholm, Quasi-fission: The mass-drift mode in heavy-ion reactions, *Nucl. Phys. A* **440**, 327 (1985).
- [24] R. du Rietz, D. J. Hinde, M. Dasgupta, R. G. Thomas, L. R. Gasques, M. Evers, N. Lobanov, and A. Wakhle, Predominant Time Scales in Fission Processes in Reactions of S, Ti and Ni with W: Zeptosecond versus Attosecond, *Phys. Rev. Lett.* **106**, 052701 (2011).
- [25] D. J. Hinde, D. Hilscher, H. Rossner, B. Gebauer, M. Lehmann, and M. Wilpert, Neutron emission as a probe of fusion-fission and quasi-fission dynamics, *Phys. Rev. C* **45**, 1229 (1992).
- [26] D. J. Hinde, M. Dasgupta, J. R. Leigh, J. P. Lestone, J. C. Mein, C. R. Morton, J. O. Newton, and H. Timmers, Fusion-Fission versus Quasifission: Effect of Nuclear Orientation, *Phys. Rev. Lett.* **74**, 1295 (1995).
- [27] M. G. Itkis, J. Äystö, S. Beghini, A. A. Bogachev, L. Corradi, O. Dorvaux, A. Gadea, G. Giardina, F. Hanappe, I. M. Itkis, M. Jandel, J. Kliman, S. V. Khlebnikov, G. N. Kniajeva, N. A. Kondratiev, E. M. Kozulin, L. Krupa, A. Latina, T. Materna, G. Montagnoli, Yu. Ts. Oganessian, I. V. Pokrovsky, E. V. Prokhorova, N. Rowley, V. A. Rubchenya, A. Ya. Rusanov, R. N. Sagaidak, F. Scarlassara, A. M. Stefanini, L. Stuttge, S. Szilner, M. Trotta, W. H. Trzaska, D. N. Vakhin, A. M. Vinodkumar, V. M. Voskressenski, and V. I. Zagrebaev, Shell effects in fission and quasi-fission of heavy and superheavy nuclei, *Nucl. Phys. A* **734**, 136 (2004).
- [28] A. Wakhle, C. Simenel, D. J. Hinde, M. Dasgupta, M. Evers, D. H. Luong, R. du Rietz, and E. Williams, Interplay between Quantum Shells and Orientation in Quasifission, *Phys. Rev. Lett.* **113**, 182502 (2014).
- [29] Z. Majka, R. Planeta, Z. Sosin, A. Wieloch, K. Zelga, M. Adamczyk, K. Pelczar, M. Barbui, S. Wuenschel, K. Hagel, X. Cao, E.-J. Kim, J. Natowitz, R. Wada, H. Zheng, G. Giuliani, and S. Kowalski, A novel experimental setup for rare events selection and its potential application to super-heavy elements search, *Acta Phys. Pol. B* **49**, 1801 (2018).
- [30] S. Wuenschel, K. Hagel, M. Barbui, J. Gauthier, X. G. Cao, R. Wada, E. J. Kim, Z. Majka, R. Planeta, Z. Sosin, A. Wieloch, K. Zelga, S. Kowalski, K. Schmidt, C. Ma, G. Zhang, and J. B. Natowitz, Experimental survey of the production of α -decaying heavy elements in $^{238}\text{U} + ^{232}\text{Th}$ reactions at 7.5–6.1 MeV/nucleon, *Phys. Rev. C* **97**, 064602 (2018).
- [31] Z.-Q. Feng, G.-M. Jin, and J.-Q. Li, Production of heavy isotopes in transfer reactions by collisions of $^{238}\text{U} + ^{238}\text{U}$, *Phys. Rev. C* **80**, 067601 (2009).
- [32] R. K. Gupta, S. K. Patra, P. D. Stevenson, and W. Greiner, A highly neutron-rich cluster and/or a superheavy nucleus in the compound nucleus $^{238}\text{U} + ^{238}\text{U}$: A mean field study, *Intl. J. Mod. Phys. E* **16**, 1721 (2007).
- [33] V. V. Sargsyan, Z. Kanokov, G. G. Adamian, N. V. Antonenko, and W. Scheid, Interaction times in the $^{136}\text{Xe} + ^{136}\text{Xe}$ and $^{238}\text{U} + ^{238}\text{U}$ reactions with a quantum master equation, *Phys. Rev. C* **80**, 047603 (2009).
- [34] K. Zhao, X. Wu, and Z. Li, Quantum molecular dynamics study of the mass distribution of products in 7.0A MeV $^{238}\text{U} + ^{238}\text{U}$ collisions, *Phys. Rev. C* **80**, 054607 (2009).
- [35] Junlong Tian, Xizhen Wu, Kai Zhao, Yingxun Zhang, and Zhuxia Li, Properties of the composite systems formed in the reactions $^{238}\text{U} + ^{238}\text{U}$ and $^{232}\text{Th} + ^{250}\text{Cf}$, *Phys. Rev. C* **77**, 064603 (2008).
- [36] R. Y. Cusson, J. A. Maruhn, and H. Stöcker, Collision of $^{238}\text{U} + ^{238}\text{U}$ using a three-dimensional TDHF-BCS model, *Z. Phys. A* **294**, 257 (1980).
- [37] A. S. Umar, C. Simenel, and W. Ye, Transport properties of isospin asymmetric nuclear matter using the time-dependent Hartree-Fock method, *Phys. Rev. C* **96**, 024625 (2017).
- [38] V. E. Oberacker, A. S. Umar, and C. Simenel, Dissipative dynamics in quasifission, *Phys. Rev. C* **90**, 054605 (2014).
- [39] K. Hammerton, Z. Kohley, D. J. Hinde, M. Dasgupta, A. Wakhle, E. Williams, V. E. Oberacker, A. S. Umar, I. P. Carter, K. J. Cook, J. Greene, D. Y. Jeung, D. H. Luong, S. D. McNeil, C. S. Palshetkar, D. C. Rafferty, C. Simenel, and K. Stiefel, Reduced quasifission competition in fusion reactions forming neutron-rich heavy elements, *Phys. Rev. C* **91**, 041602 (2015).
- [40] A. S. Umar and V. E. Oberacker, Time-dependent HF approach to SHE dynamics, *Nucl. Phys. A* **944**, 238 (2015).
- [41] A. S. Umar, V. E. Oberacker, and C. Simenel, Fusion and quasifission dynamics in the reactions $^{48}\text{Ca} + ^{249}\text{Bk}$ and $^{50}\text{Ti} + ^{249}\text{Bk}$ using a time-dependent Hartree-Fock approach, *Phys. Rev. C* **94**, 024605 (2016).
- [42] K. Godbey, A. S. Umar, and C. Simenel, Deformed shell effects in $^{48}\text{Ca} + ^{249}\text{Bk}$ quasifission fragments, *Phys. Rev. C* **100**, 024610 (2019).
- [43] C. Simenel and A. S. Umar, Formation and dynamics of fission fragments, *Phys. Rev. C* **89**, 031601 (2014).
- [44] G. Scamps, C. Simenel, and D. Lacroix, Superfluid dynamics of ^{258}Fm fission, *Phys. Rev. C* **92**, 011602 (2015).
- [45] P. M. Goddard, P. D. Stevenson, and A. Rios, Fission dynamics within time-dependent Hartree-Fock: deformation-induced fission, *Phys. Rev. C* **92**, 054610 (2015).
- [46] Y. Tanimura, D. Lacroix, and G. Scamps, Collective aspects deduced from time-dependent microscopic mean-field with pairing: Application to the fission process, *Phys. Rev. C* **92**, 034601 (2015).
- [47] P. M. Goddard, P. D. Stevenson, and A. Rios, Fission dynamics within time-dependent Hartree-Fock. II. Boost-induced fission, *Phys. Rev. C* **93**, 014620 (2016).
- [48] Aurel Bulgac, Piotr Magierski, Kenneth J. Roche, and Ionel Stetcu, Induced Fission of ^{240}Pu within a Real-Time Microscopic Framework, *Phys. Rev. Lett.* **116**, 122504 (2016).
- [49] Y. Tanimura, D. Lacroix, and S. Ayik, Microscopic Phase-Space Exploration Modeling of ^{258}Fm Spontaneous Fission, *Phys. Rev. Lett.* **118**, 152501 (2017).
- [50] G. Scamps and C. Simenel, Impact of pear-shaped fission fragments on mass-asymmetric fission in actinides, *Nature* **564**, 382 (2018).
- [51] Aurel Bulgac, Michael McNeil Forbes, Shi Jin, Rodrigo Navarro Perez, and Nicolas Schunck, Minimal nuclear energy density functional, *Phys. Rev. C* **97**, 044313 (2018).
- [52] G. Scamps and C. Simenel, Effect of shell structure on the fission of sub-lead nuclei, *Phys. Rev. C* **100**, 041602 (2019).
- [53] C. Simenel and A. S. Umar, Heavy-ion collisions and fission dynamics with the time-dependent Hartree-Fock theory and its extensions, *Prog. Part. Nucl. Phys.* **103**, 19 (2018).
- [54] Kazuyuki Sekizawa, TDHF Theory and Its Extensions for the Multinucleon Transfer Reaction: A Mini Review, *Front. Phys.* **7**, 20 (2019).
- [55] Yu. Ts. Oganessian, Private Communication (2018).
- [56] J. W. Negele, The mean-field theory of nuclear-structure and dynamics, *Rev. Mod. Phys.* **54**, 913 (1982).
- [57] C. Simenel, Nuclear quantum many-body dynamics, *Eur. Phys. J. A* **48**, 152 (2012).
- [58] P. Bonche, B. Grammaticos, and S. Koonin, Three-dimensional time-dependent Hartree-Fock calculations of $^{16}\text{O} + ^{16}\text{O}$ and $^{40}\text{Ca} + ^{40}\text{Ca}$ fusion cross sections, *Phys. Rev. C* **17**, 1700 (1978).
- [59] H. Flocard, S. E. Koonin, and M. S. Weiss, Three-dimensional

- time-dependent Hartree-Fock calculations: Application to $^{16}\text{O} + ^{16}\text{O}$ collisions, *Phys. Rev. C* **17**, 1682 (1978).
- [60] C. Simenel, P. Chomaz, and G. de France, Quantum Calculation of the Dipole Excitation in Fusion Reactions, *Phys. Rev. Lett.* **86**, 2971 (2001).
- [61] A. S. Umar and V. E. Oberacker, Time dependent Hartree-Fock fusion calculations for spherical, deformed systems, *Phys. Rev. C* **74**, 024606 (2006).
- [62] Kouhei Washiyama and Denis Lacroix, Energy dependence of the nucleus-nucleus potential close to the Coulomb barrier, *Phys. Rev. C* **78**, 024610 (2008).
- [63] A. S. Umar, V. E. Oberacker, J. A. Maruhn, and P.-G. Reinhard, Entrance channel dynamics of hot and cold fusion reactions leading to superheavy elements, *Phys. Rev. C* **81**, 064607 (2010).
- [64] A. S. Umar, V. E. Oberacker, J. A. Maruhn, and P.-G. Reinhard, Microscopic calculation of precompound excitation energies for heavy-ion collisions, *Phys. Rev. C* **80**, 041601 (2009).
- [65] Lu Guo and Takashi Nakatsukasa, Time-dependent Hartree-Fock studies of the dynamical fusion threshold, *EPJ Web Conf.* **38**, 09003 (2012).
- [66] R. Kesper, A. S. Umar, and V. E. Oberacker, Microscopic study of Ca+Ca fusion, *Phys. Rev. C* **85**, 044606 (2012).
- [67] C. Simenel, R. Kesper, A. S. Umar, and V. E. Oberacker, Microscopic study of $^{16}\text{O} + ^{16}\text{O}$ fusion, *Phys. Rev. C* **88**, 024617 (2013).
- [68] V. E. Oberacker, A. S. Umar, J. A. Maruhn, and P.-G. Reinhard, Dynamic microscopic study of pre-equilibrium giant resonance excitation and fusion in the reactions $^{132}\text{Sn} + ^{48}\text{Ca}$ and $^{124}\text{Sn} + ^{40}\text{Ca}$, *Phys. Rev. C* **85**, 034609 (2012).
- [69] V. E. Oberacker, A. S. Umar, J. A. Maruhn, and P. Reinhard, Microscopic study of the $^{132,124}\text{Sn} + ^{96}\text{Zr}$ reactions: Dynamic excitation energy, energy-dependent heavy-ion potential, and capture cross section, *Phys. Rev. C* **82**, 034603 (2010).
- [70] A. S. Umar, V. E. Oberacker, and C. J. Horowitz, Microscopic sub-barrier fusion calculations for the neutron star crust, *Phys. Rev. C* **85**, 055801 (2012).
- [71] C. Simenel, M. Dasgupta, D. J. Hinde, and E. Williams, Microscopic approach to coupled-channels effects on fusion, *Phys. Rev. C* **88**, 064604 (2013).
- [72] A. S. Umar, C. Simenel, and V. E. Oberacker, Energy dependence of potential barriers and its effect on fusion cross sections, *Phys. Rev. C* **89**, 034611 (2014).
- [73] X. Jiang, J. A. Maruhn, and S. Yan, Microscopic study of non-central effects in heavy-ion fusion reactions with spherical nuclei, *Phys. Rev. C* **90**, 064618 (2014).
- [74] S. E. Koonin, K. T. R. Davies, V. Maruhn-Rezwani, H. Feldmeier, S. J. Krieger, and J. W. Negele, Time-dependent Hartree-Fock calculations for $^{16}\text{O} + ^{16}\text{O}$ and $^{40}\text{Ca} + ^{40}\text{Ca}$ reactions, *Phys. Rev. C* **15**, 1359 (1977).
- [75] C. Simenel, Particle Transfer Reactions with the Time-Dependent Hartree-Fock Theory Using a Particle Number Projection Technique, *Phys. Rev. Lett.* **105**, 192701 (2010).
- [76] C. Simenel, Particle-Number Fluctuations and Correlations in Transfer Reactions Obtained Using the Balian-Vénéroni Variational Principle, *Phys. Rev. Lett.* **106**, 112502 (2011).
- [77] Kazuyuki Sekizawa and Kazuhiro Yabana, Time-dependent Hartree-Fock calculations for multinucleon transfer processes in $^{40,48}\text{Ca} + ^{124}\text{Sn}$, $^{40}\text{Ca} + ^{208}\text{Pb}$, and $^{58}\text{Ni} + ^{208}\text{Pb}$ reactions, *Phys. Rev. C* **88**, 014614 (2013).
- [78] G. Scamps and D. Lacroix, Effect of pairing on one- and two-nucleon transfer below the Coulomb barrier: A time-dependent microscopic description, *Phys. Rev. C* **87**, 014605 (2013).
- [79] K. Sekizawa and K. Yabana, Particle-number projection method in time-dependent Hartree-Fock theory: Properties of reaction products, *Phys. Rev. C* **90**, 064614 (2014).
- [80] D. Bourgin, C. Simenel, S. Courtin, and F. Haas, Microscopic study of $^{40}\text{Ca} + ^{58,64}\text{Ni}$ fusion reactions, *Phys. Rev. C* **93**, 034604 (2016).
- [81] C. Bottcher, M. R. Strayer, A. S. Umar, and P.-G. Reinhard, Damped relaxation techniques to calculate relativistic bound-states, *Phys. Rev. A* **40**, 4182 (1989).
- [82] A. S. Umar and V. E. Oberacker, Three-dimensional unrestricted time-dependent Hartree-Fock fusion calculations using the full Skyrme interaction, *Phys. Rev. C* **73**, 054607 (2006).
- [83] J. A. Maruhn, P.-G. Reinhard, P. D. Stevenson, and A. S. Umar, The TDHF Code Sky3D, *Comput. Phys. Commun.* **185**, 2195 (2014).
- [84] Roger Balian and Marcel Vénéroni, Time-Dependent Variational Principle for Predicting the Expectation Value of an Observable, *Phys. Rev. Lett.* **47**, 1353 (1981).
- [85] C. H. Dasso, T. Dossing, and H. C. Pauli, On the mass distribution in Time-Dependent Hartree-Fock calculations of heavy-ion collisions, *Z. Phys. A* **289**, 395 (1979).
- [86] S. Ayik, A stochastic mean-field approach for nuclear dynamics, *Phys. Lett. B* **658**, 174 (2008).
- [87] D. Lacroix and S. Ayik, Stochastic quantum dynamics beyond mean field, *Eur. Phys. J. A* **50**, 95 (2014).
- [88] Roger Balian and Marcel Vénéroni, Fluctuations in a time-dependent mean-field approach, *Phys. Lett. B* **136**, 301 (1984).
- [89] J. M. A. Broomfield, *Calculations of Mass Distributions using the Balian-Vénéroni Variational Approach*, Ph.D. thesis, University of Surrey, Guildford, United Kingdom (2009).
- [90] E. Williams, K. Sekizawa, D. J. Hinde, C. Simenel, M. Dasgupta, I. P. Carter, K. J. Cook, D. Y. Jeung, S. D. McNeil, C. S. Palshetkar, D. C. Rafferty, K. Ramachandran, and A. Wakhle, Exploring Zeptosecond Quantum Equilibration Dynamics: From Deep-Inelastic to Fusion-Fission Outcomes in $^{58}\text{Ni} + ^{60}\text{Ni}$ Reactions, *Phys. Rev. Lett.* **120**, 022501 (2018).
- [91] P. Bonche and H. Flocard, Dispersion of one-body operators with the Balian-Veneroni variational principle, *Nucl. Phys. A* **437**, 189 (1985).
- [92] Ka-Hae Kim, Takaharu Otsuka, and Paul Bonche, Three-dimensional TDHF calculations for reactions of unstable nuclei, *J. Phys. G* **23**, 1267 (1997).
- [93] A. S. Umar, M. R. Strayer, J. S. Wu, D. J. Dean, and M. C. Güçlü, Nuclear Hartree-Fock calculations with splines, *Phys. Rev. C* **44**, 2512 (1991).
- [94] Y. Fu, H. Tong, X. F. Wang, H. Wang, D. Q. Wang, X. Y. Wang, and J. M. Yao, Microscopic analysis of shape transition in neutron-deficient Yb isotopes, *Phys. Rev. C* **97**, 014311 (2018).
- [95] K. Nomura, T. Otsuka, R. Rodríguez-Guzmán, L. M. Robledo, and P. Sarriguren, Collective structural evolution in neutron-rich Yb, Hf, W, Os, and Pt isotopes, *Phys. Rev. C* **84**, 054316 (2011).
- [96] L. M. Robledo, R. Rodríguez-Guzmán, and P. Sarriguren, Role of triaxiality in the ground-state shape of neutron-rich Yb, Hf, W, Os and Pt isotopes, *J. Phys. G* **36**, 115104 (2009).
- [97] P. Sarriguren, R. Rodríguez-Guzmán, and L. M. Robledo, Shape transitions in neutron-rich Yb, Hf, W, Os, and Pt isotopes within a Skyrme Hartree-Fock + BCS approach, *Phys. Rev. C* **77**, 064322 (2008).
- [98] C. Xu, H. Hua, X. Q. Li, J. Meng, Z. H. Li, F. R. Xu, Y. Shi, H. L. Liu, S. Q. Zhang, Z. Y. Li, L. H. Zhu, X. G. Wu, G. S.

- Li, C. Y. He, S. G. Zhou, S. Y. Wang, Y. L. Ye, D. X. Jiang, T. Zheng, J. L. Lou, L. Y. Ma, E. H. Wang, Y. Y. Cheng, and C. He, New insight into the shape coexistence and shape evolution of ^{157}Yb , *Phys. Rev. C* **83**, 014318 (2011).
- [99] Cédric Simenel and Benoit Avez, Time-dependent Hartree-Fock description of heavy ions fusion, *Intl. J. Mod. Phys. E* **17**, 31 (2008).
- [100] C. Simenel, A. S. Umar, K. Godbey, M. Dasgupta, and D. J. Hinde, How the Pauli exclusion principle affects fusion of atomic nuclei, *Phys. Rev. C* **95**, 031601 (2017).
- [101] W. Q. Shen, J. Albinski, A. Gobbi, S. Gralla, K. D. Hildenbrand, N. Herrmann, J. Kuzminski, W. F. J. Müller, H. Stelzer, J. Töke, B. B. Back, S. Bjørnholm, and S. P. Sørensen, Fission and quasifission in U-induced reactions, *Phys. Rev. C* **36**, 115 (1987).
- [102] D. J. Hinde, R. G. Thomas, R. du Rietz, A. Diaz-Torres, M. Dasgupta, M. L. Brown, M. Evers, L. R. Gasques, R. Rafiei, and M. D. Rodriguez, Disentangling Effects of Nuclear Structure in Heavy Element Formation, *Phys. Rev. Lett.* **100**, 202701 (2008).
- [103] C. Simenel, D. J. Hinde, R. du Rietz, M. Dasgupta, M. Evers, C. J. Lin, D. H. Luong, and A. Wakhle, Influence of entrance-channel magicity and isospin on quasi-fission, *Phys. Lett. B* **710**, 607 (2012).
- [104] R. du Rietz, E. Williams, D. J. Hinde, M. Dasgupta, M. Evers, C. J. Lin, D. H. Luong, C. Simenel, and A. Wakhle, Mapping quasifission characteristics and timescales in heavy element formation reactions, *Phys. Rev. C* **88**, 054618 (2013).
- [105] M. Morjean, D. J. Hinde, C. Simenel, D. Y. Jeung, M. Airiau, K. J. Cook, M. Dasgupta, A. Drouart, D. Jacquet, S. Kalkal, C. S. Palshetkar, E. Prasad, D. Rafferty, E. C. Simpson, L. Tassan-Got, K. Vo-Phuoc, and E. Williams, Evidence for the Role of Proton Shell Closure in Quasifission Reactions from X-Ray Fluorescence of Mass-Identified Fragments, *Phys. Rev. Lett.* **119**, 222502 (2017).
- [106] G. Mohanto, D. J. Hinde, K. Banerjee, M. Dasgupta, D. Y. Jeung, C. Simenel, E. C. Simpson, A. Wakhle, E. Williams, I. P. Carter, K. J. Cook, D. H. Luong, C. S. Palshetkar, and D. C. Rafferty, Interplay of spherical closed shells and N/Z asymmetry in quasifission dynamics, *Phys. Rev. C* **97**, 054603 (2018).
- [107] D. J. Hinde, D. Y. Jeung, E. Prasad, A. Wakhle, M. Dasgupta, M. Evers, D. H. Luong, R. du Rietz, C. Simenel, E. C. Simpson, and E. Williams, Sub-barrier quasifission in heavy element formation reactions with deformed actinide target nuclei, *Phys. Rev. C* **97**, 024616 (2018).
- [108] K. Sekizawa and K. Yabana, Time-dependent Hartree-Fock calculations for multinucleon transfer and quasifission processes in the $^{64}\text{Ni} + ^{238}\text{U}$ reaction, *Phys. Rev. C* **93**, 054616 (2016).
- [109] Edward Simpson, *The Colourful Nuclide Chart*, Tech. Rep. (Australian National University, 2019).
- [110] I. M. Itkis, E. M. Kozulin, M. G. Itkis, G. N. Knyazheva, A. A. Bogachev, E. V. Chernysheva, L. Krupa, Yu. Ts. Oganessian, V. I. Zagrebaev, A. Ya. Rusanov, F. Goennenwein, O. Dorvaux, L. Stuttgé, F. Hanappe, E. Vardaci, and E. Goés de Brenand, Fission and quasifission modes in heavy-ion-induced reactions leading to the formation of Hs^* , *Phys. Rev. C* **83**, 064613 (2011).
- [111] M. G. Itkis, E. Vardaci, I. M. Itkis, G. N. Knyazheva, and E. M. Kozulin, Fusion and fission of heavy and superheavy nuclei (experiment), *Nucl. Phys. A* **944**, 204 (2015).
- [112] E. M. Kozulin, G. N. Knyazheva, T. K. Ghosh, A. Sen, I. M. Itkis, M. G. Itkis, K. V. Novikov, I. N. Diatlov, I. V. Pchelintsev, C. Bhattacharya, S. Bhattacharya, K. Banerjee, E. O. Saveleva, and I. V. Vorobiev, Fission and quasifission of the composite system $Z = 114$ formed in heavy-ion reactions at energies near the coulomb barrier, *Phys. Rev. C* **99**, 014616 (2019).
- [113] K. Banerjee, D. J. Hinde, M. Dasgupta, E. C. Simpson, D. Y. Jeung, C. Simenel, B. M. A. Swinton-Bland, E. Williams, I. P. Carter, K. J. Cook, H. M. David, C. Düllmann, J. Khuyagbaatar, B. Kindler, B. Lommel, E. Prasad, C. Sengupta, J. F. Smith, K. Vo-Phuoc, J. Walshe, and A. Yakushev, Mechanisms Suppressing Superheavy Element Yields in Cold Fusion Reactions, *Phys. Rev. Lett.* **122**, 232503 (2019).
- [114] R. G. Thomas, D. J. Hinde, D. Duniec, F. Zenke, M. Dasgupta, M. L. Brown, M. Evers, L. R. Gasques, M. D. Rodriguez, and A. Diaz-Torres, Entrance channel dependence of quasifission in reactions forming ^{220}Th , *Phys. Rev. C* **77**, 034610 (2008).
- [115] K. Sekizawa, Microscopic description of production cross sections including deexcitation effects, *Phys. Rev. C* **96**, 014615 (2017).
- [116] A. Bulgac, S. Jin, and I. Stetcu, Unitary evolution with fluctuations and dissipation, *Phys. Rev. C* **100**, 014615 (2019).